CCM and DCM Analysis of quasi-Z-Source Inverter

Jonah Ong Soon Xuan, Kentrick Yong Sut Khan, Dr. Law Kah Haw, Dr. Wendy Ng Pei Qin
Department of Electrical and Computer Engineering
Curtin University Malaysia
jonahosx25@gmail.com, kentrick6587@live.com,
lawkahhaw@curtin.edu.my, wendyngpq@curtin.edu.my

Dr. Mohamed Dahidah
School of Engineering Merz Court
Newcastle University
Newcastle Upon Tyne NE1 7RU, UK
mohamed.dahidah@ncl.ac.uk

***Abstract*— This paper presents an analysis of a quasi-Z-source inverter (qZSI) operating in continuous conduction mode (CCM) and discontinuous conduction mode (DCM). The boundary between CCM and DCM is discovered and technique to avoid qZSI being operated in DCM is also discovered. The analysis concluded an equation that provides the minimum inductor current and the inductance before qZSI enters DCM. Additionally, the relationship between input and DC-link voltages in DCM is also presented with valid mathematical derivation. A qZSI model is being simulated using MATLAB/SIMULINK® to verify the proposed technique. The simulated results meet the analysis results very well. The design of qZSI for application like photovoltaic (PV), wind power and distributed generations (DG) can be achieved with broad versatility.**

***Index Terms*— quasi-Z-source inverter (qZSI), continuous conduction mode (CCM), discontinuous conduction mode (DCM)**

I. Introduction

The qZSI is originated from Z-source inverter (ZSI). ZSI and qZSI were invented in 2003 and 2008 respectively [1]. The emergence of ZSI incited researchers to further improve the circuit topology and later was advanced to be called a qZSI shown in Fig. 1 [1].

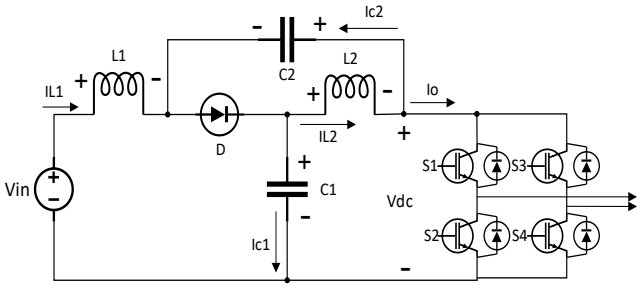

Fig. 1. qZSI topology

The specialty of qZSI is that it possesses the capability to step-up or step-down DC voltages in a single-stage control scheme. This feature outperforms the characteristic of a traditional voltage source inverter (VSI) whereby an extra DC-DC converter is needed to buck or boost the DC source voltage to yield the desired DC-link voltage which then to be inverted into the AC form. Such control scheme involves two stages, one for the DC-DC converter, the other for the DC to AC inversion [1].

The advantage of qZSI over the traditional VSI is lesser cost and the implementation of simpler control method due to its single-stage control scheme. This means that qZSI does not need additional switches to fully operate; only the switches at the inverter side with modified control algorithm are adequate to achieve its buck/boost functions [2].

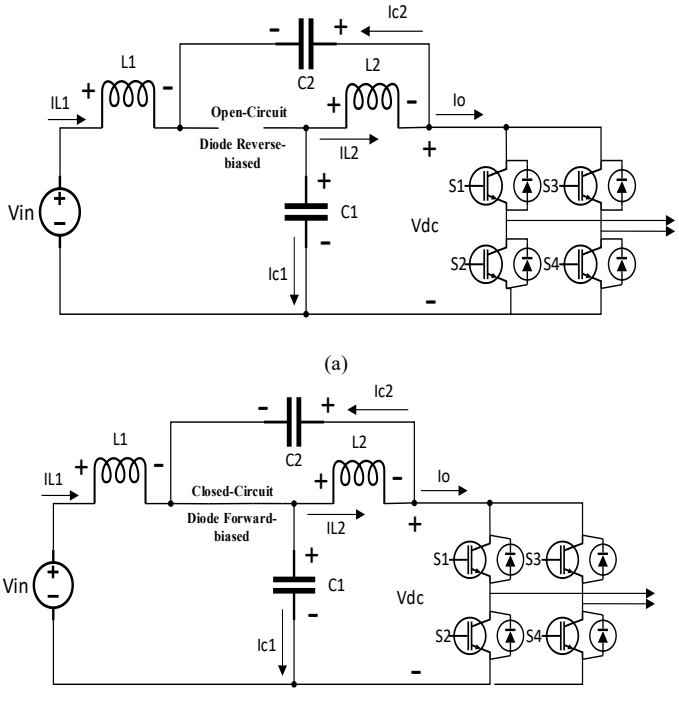

Fig. 2. (a) qZSI in shoot-through state. (b) qZSI in non-shoot-thought state

As shown in Fig. 2, qZSI has the advantage of operating in shoot-through state whereby the phase leg of the inverter is short-circuited by turning on two switches simultaneously without the dead time [1]. The shoot-through state is tolerable in qZSI but forbidden in the traditional VSI because the inductors in the quasi-Z-source (qZS) network are charged up by the capacitors during the shoot-through state without short-circuiting them [3]. Hence, the increase in magnetic energy stored in the inductor will provide the voltage boost effect during the non-shoot-through state. All in all, if the shoot-through duty cycle is controlled properly, qZSI can fulfill boost or buck effect to achieve the desired DC-link voltage for DC to AC inversion [3].

Consequently, the availability of qZSI to operate in shoot-through state makes it very useful in handling input sources whose voltages vary in a wide range that are needed to be stepped-up, maintained and fed into the grid such as fuel cells, photovoltaic modules and distributed generations (DGs) [4]. With the emergence and advancement of qZSI in the realm of power electronics, it sets to replace the conventional two-stage

DC-DC converter connected in series with H-bridge inverter with a great cost reduction and improved performance [4].

Based on the aforementioned, because of the ability to shoot-through, the DC-link voltage, V_{dc} is boosted with a boost factor, β. This V_{dc} which is the output of the qZS network, serves as the input for the inverter side. With the boosted V_{dc}, the inverter can achieve high AC voltages to meet desired voltage levels of real-life applications [1]. Therefore, the factor term governing the relationship between qZSI input voltage, V_{in} and the output rms inverter voltage, v_{ac_rms} is called the voltage gain, *G* [5]. The boost factor, β and the voltage gain *G* are defined as

$$\beta = \frac{V_{dc}}{V_{in}} = \frac{1}{1-2D} \tag{1}$$

$$G = \frac{v_{ac\_rms}}{V_{in}} = MB \tag{2}$$

where *D* is the shoot-through duty ratio and M is the modulation index;

$$M = \frac{A_m}{A_c} \tag{3}$$

where A_m is the modulation amplitude and A_c is the carrier amplitude.

From (1), *D* cannot be more than 0.5 as it will send the quotient to infinity because the denominator is zero. Thus, it is important to always keep the shoot-through duty ratio less than 0.5 [1]. To know how the above equations are obtained requires mathematical derivations which will be discussed.

On the other hand, the two main modulation techniques are called sinusoidal pulse width modulation (SPWM) and space vector pulse width modulation (SVPWM). Because of the requirement of shoot-through state, SPWM in qZSI has three different modes namely, the simple boost control (SBC), maximum boost control (MBC) and maximum constant boost control (MCBC) [1],[6]. The modification made to the traditional SPWM involves adding the top and lower shoot-through references v_p and v_n respectively [1]. When carrier waveform is higher than the v_p or when carrier waveform is lower than the v_n, the resulting gate signals make the qZSI to shoot-through [1].

II. CCM AND DCM ANALYSIS OF QZSI

CCM and DCM are relevant to qZSI because the circuitry internally consists of a dc-dc voltage boost structure with inductors and capacitors inherently present [7]. Therefore, CCM and DCM will affect the performance of qZSI. The equations governing the qZSI mentioned in the previous sections are considered valid only in CCM. Nevertheless, should the qZSI operates in DCM, analysis and calculations are required to formulate the corresponding governing equations [8]. Thus, CCM and DCM operations are crucial to be considered in designing qZSI to yield the desirable results [9]. qZSI network has the input inductor that buffers the source current of the network. Therefore, the qZS network can operate in CCM when the input current never drops to zero during shoot-through state. With CCM operation, the input voltage stress can be minimized, which is important in power electronics applications. CCM and DCM control schemes for boost converter had been proposed by Shu et.al in 2011 at which the DCM control can be achieved with minimal changes to the CCM average current control structure [10]. When load decreases, the converters enters into DCM mode even if the inductance is large. In other words, the converter transits from DCM to CCM or vice versa under a large load change. Numeric state-space-average value models of PWM DC-DC converters have been derived and proposed in [11]. Ultimately, only few works had been done in comprehensive mathematical analysis between DCM and CCM of the qZSI. In [9], [12], CCM and DCM of a cascaded-qZS were analyzed and the techniques to avoid undesirable DCM operation were also discussed in the works. Nevertheless, no existing work has been done to analyze DCM and CCM in conventional qZSI. Hence, this is the objective of this paper.

A. Operation Analysis in CCM

The CCM operating state of the qZSI in one switching cycle consists of shoot-through state and non-shoot-through state.

$$T_S = D_{sh} + D_{nsh} \tag{4}$$

D_{sh} represents shoot-through duty ratio while D_{nsh} or $(1 - D_{sh})$ represents non-shoot-through duty ratio.

Through circuit analysis on the equivalent circuit of qZSI in shoot-through state shown in Fig. 2(a), a first-order differential equation involving the inductor-1 voltage, V_{L1}, inductor-2 voltage, V_{L2}, capacitor-1 current, I_{C1}, capacitor-2 current, I_{C2}, input voltage, V_{in} and output dc current I_o are shown in matrix form below. *Note: $V_L = \mathrm{L}\frac{dI_L}{dt}$, $I_C = \mathrm{C}\frac{dV_C}{dt}$.

$$\begin{bmatrix} L_1 & 0 & 0 & 0 \\ 0 & L_2 & 0 & 0 \\ 0 & 0 & C_1 & 0 \\ 0 & 0 & 0 & C_2 \end{bmatrix} \begin{bmatrix} i_{L1}^{\cdot}(t) \\ i_{L2}^{\cdot}(t) \\ v_{C1}^{\cdot}(t) \\ v_{C2}^{\cdot}(t) \end{bmatrix} = \begin{bmatrix} 0 & 0 & 0 & 1 \\ 0 & 0 & 1 & 0 \\ 0 & -1 & 0 & 0 \\ -1 & 0 & 0 & 0 \end{bmatrix} \begin{bmatrix} i_{L1}(t) \\ i_{L2}(t) \\ v_{C1}(t) \\ v_{C2}(t) \end{bmatrix} + \begin{bmatrix} 1 & 0 \\ 0 & 0 \\ 0 & 0 \\ 0 & 0 \end{bmatrix} \begin{bmatrix} v_{in}(t) \\ i_o(t) \end{bmatrix} \tag{5}$$

In shoot-through state, the DC-link voltage, $V_{dc} = 0$.

Through circuit analysis on the equivalent circuit of qZSI in non-shoot-through state shown in Fig. 2(b), the corresponding matrix form is shown in (6).

$$\begin{bmatrix} L_1 & 0 & 0 & 0 \\ 0 & L_2 & 0 & 0 \\ 0 & 0 & C_1 & 0 \\ 0 & 0 & 0 & C_2 \end{bmatrix} \begin{bmatrix} i_{L1}^{\cdot}(t) \\ i_{L2}^{\cdot}(t) \\ v_{C1}^{\cdot}(t) \\ v_{C2}^{\cdot}(t) \end{bmatrix} = \begin{bmatrix} 0 & 0 & -1 & 0 \\ 0 & 0 & 0 & -1 \\ 1 & 0 & 0 & 0 \\ 0 & 1 & 0 & 0 \end{bmatrix} \begin{bmatrix} i_{L1}(t) \\ i_{L2}(t) \\ v_{C1}(t) \\ v_{C2}(t) \end{bmatrix} + \begin{bmatrix} 1 & 0 \\ 0 & 0 \\ 0 & -1 \\ 0 & -1 \end{bmatrix} \begin{bmatrix} v_{in}(t) \\ i_o(t) \end{bmatrix} \tag{6}$$

In non-shoot-through state, $V_{dc} = V_{C1} + V_{C2}$.

Based on inductor volt-second balance (IVSB) and capacitor ampere-second balance (CASB), in transition of both shoot-through and non-shoot-through states, the current

flowing through the inductor cannot change instantaneously. Same goes to voltage across the capacitor cannot change instantaneously. Hence, in steady-state condition, the average voltage across the inductor and the average current flowing through the capacitor in one switching cycle are equal to zero.

$$\langle V_{L1}\rangle = D_{sh}T_s(V_{in}+V_{C2}) + D_{nsh}T_s(V_{in}-V_{C1}) \quad (7)$$

$$\langle V_{L2}\rangle = D_{sh}T_s(V_{C1}) + D_{nsh}T_s(-V_{C2}) \quad (8)$$

$$\langle I_{C1}\rangle = D_{sh}T_s(-i_{L2}) + D_{nsh}T_s(i_{L1}-i_O) \quad (9)$$

$$\langle I_{C2}\rangle = D_{sh}T_s(-i_{L1}) + D_{nsh}T_s(i_{L2}-i_O) \quad (10)$$

By equating the equations above to zero, the steady-state inductor current relationship, the input voltage, the capacitor voltages and the DC-link voltages with respect to D_{sh} are obtained.

$$I_{L1} = I_{L2} = \frac{P}{V_{in}} = \frac{(MV_{dc})^2}{V_{in}R} \quad (11)$$

$$\frac{V_{C1}}{V_{in}} = \frac{(1-D_{sh})}{(1-2D_{sh})} \quad (12)$$

$$\frac{V_{C2}}{V_{in}} = \frac{D_{sh}}{(1-2D_{sh})} \quad (13)$$

$$\frac{V_{DC}}{V_{in}} = \beta = \frac{1}{(1-2D_{sh})} \quad (14)$$

P is the power rating of the qZSI. For an ideal power converter, $P_{in} = P_{out}$ and R is the load resistance.

B. *Operation Analysis at the Boundary of CCM and DCM*

In *Section A,* the voltages across both inductors are analyzed. Because current flowing through the inductor cannot change immediately, the shoot-through characteristics of the qZSI will render a ripple effect on the inductor current. The ripple currents flowing through both the inductors are denoted by ΔI_{L1} and ΔI_{L2}. Note that analysis is done in the assumption of a steady-state whereby the inductor current increases, $\Delta I_L(+)$ during the D_{sh} state must be the equal to the decrease $\Delta I_L(-)$ during the D_{nsh} state.

In CCM, the inductor current is continuous in an up-down adjoining line; seemingly like a triangular-shaped graph. At the boundary between CCM and DCM, the ripple inductor current falls upon touching the x-axis. The trailing statements are clearly depicted in Fig. 3. Hence, ΔI_{L1} and ΔI_{L2} are obtained as follow where L is the inductance, assuming $L_1 = L_2$ and f_{sw} is the switching frequency,

$$\Delta I_{L1} = \frac{1}{L}\int_0^{t_{sh}=D_{sh}T_s} V_{L1}dt = \frac{1}{L}\int_{t_{nsh}=D_{sh}T_s}^{T_s} V_{L1}dt$$
$$\Delta I_{L1} = \frac{(V_{in}+V_{C2})(D_{sh})}{Lf_{sw}} \quad (15)$$

$$\Delta I_{L2} = \frac{1}{L}\int_0^{t_{sh}=D_{sh}T_s} V_{L2}dt = \frac{1}{L}\int_{t_{nsh}=D_{sh}T_s}^{T_s} V_{L2}dt$$
$$\Delta I_{L2} = \frac{(V_{C1})(D_{sh})}{Lf_{sw}} \quad (16)$$

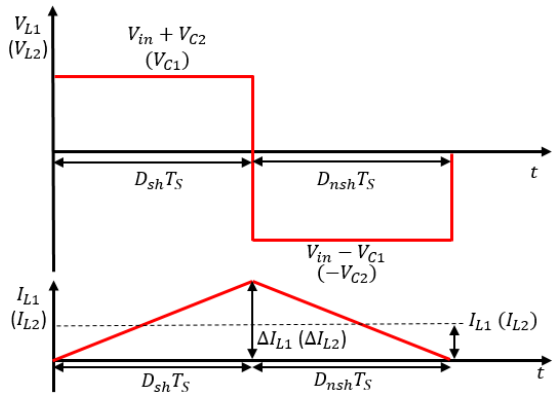

Fig. 3. Inductor voltage and current waveforms at boundary between CCM and DCM.

Based on Fig. 3 above, the boundary inductor current, I_{LB} is half the ripple current as per (17).

$$I_{LB} = \frac{1}{2}\Delta I_L \quad (17)$$

Since, it was proven in *Section A* that $I_{L1} = I_{L2}$ in steady-state, substituting (15) and (16) into (17), the boundary inductor-1 and inductor-2 currents are equated as below.

$$I_{LB1} = I_{LB2} = \frac{(V_{in}+V_{C2})(D_{sh})}{2Lf_{sw}} = \frac{(V_{C1})(D_{sh})}{2Lf_{sw}} \quad (18)$$

In [13], the power converter operates in CCM when $I_L \geq I_{LB}$ and in DCM when $I_L < I_{LB}$. Therefore, to ensure the qZSI to operate in CCM, the following equations must be fulfilled.

$$I_{LB} \geq \frac{(V_{in}+V_{C2})(D_{sh})}{2Lf_{sw}} OR \frac{(V_{C1})(D_{sh})}{2Lf_{sw}} \quad (19)$$

$$L \geq \frac{(V_{in}+V_{C2})(D_{sh})}{2I_{LB}f_{sw}} OR \frac{(V_{C1})(D_{sh})}{2I_{LB}f_{sw}} \quad (20)$$

Hence, for inductor of known inductance, L, the minimum inductor current before qZSI enters DCM is justified in (31).

$$I_{LB\_min} = \frac{(V_{in}+V_{C2})(D_{sh})}{2Lf_{sw}} \; OR \; \frac{(V_{C1})(D_{sh})}{2Lf_{sw}} \quad (21)$$

C. *Operation Analysis in DCM*

Knowing that in DCM, the qZSI steady-state voltage conversion relationship as shown in (1) no longer holds. The formulated voltage conversion relationship in DCM can be achieved by analyzing the DCM inductor current waveform as shown in Fig. 4.

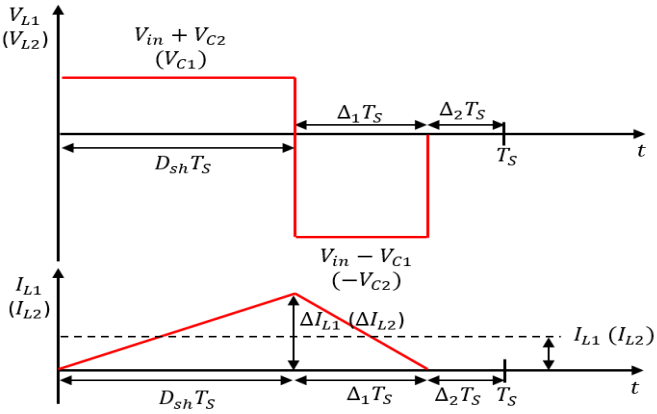

Fig. 4. Inductor voltage and current waveforms in DCM

The difference is that the D_{nsh} state is replaced by the notation, ΔT_s as compared to $D_{sh}T_s$ in CCM analysis. Hence, referring to (15) or (16), I_L becomes as follow.

$$I_L = \frac{1}{2} \times \frac{1}{T_s} \times \Delta I_L \times \left(D_{sh}T_s + \frac{V_{in} + V_{C2}}{V_{in} - V_{C1}} D_{sh}T_s\right) \quad (22)$$

Finally, substituting (11), (12), and (13) into (22) and solve for V_{dc}/V_{in},

$$\frac{V_{dc}}{V_{in}} = \frac{D_{sh}}{1 - D_{sh}} \sqrt{\frac{R}{2Lf_{sw}} \left(\frac{D_{sh} - 1}{D_{sh}}\right)} \quad (23)$$

After performing mathematical calculations, it can be concluded that in DCM, the voltage conversion relationship is a function of not only the V_{in} and D_{sh} but also involving the L and R. Consequently, the transition of the qZSI operating from CCM to DCM is primarily dependent on the load, R and the inductance, L of the inductor.

Fig. 5 below shows the boundary between DCM and CCM as a function of L, f_{sw}, I_o, V_{in} and D_{sh}. The qZSI output voltage and current relationships are shown below.

$$V_{o,rms} = \frac{MV_{dc}}{\sqrt{2}}$$
$$I_{o,rms} = \frac{I_{o,peak}}{\sqrt{2}} \quad (24)$$

Using (14), (18) and (24) and assuming M = 1, equation (25) is obtained below to justify the graph in Fig. 5.

$$\frac{Lf_{sw}I_o}{V_{in}} = D - D^2 \quad (25)$$

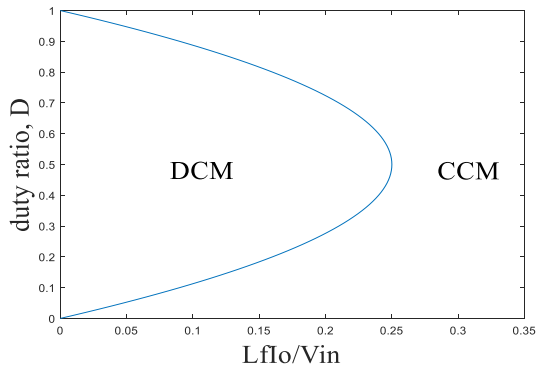

Fig. 5. DCM-CCM Boundary Transition for qZSI.

III. Simulation and Discussion

To verify the above inferences on CCM and DCM of the qZSI, the mathematical derivations are put into test by simulating a set of system parameters using MATLAB/SIMULINK® as shown in Fig. 6. The system parameters used for simulation are tabulated in Table I. Note that the qZSI being simulated is using Simple Boost Control (SBC) and triangular-carrier sinusoidal pulse width modulation (SPWM) as shown in Fig. 7 [1].

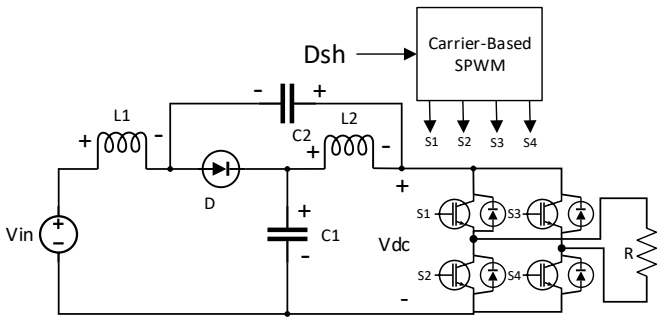

Fig. 6. MATLAB/SIMULINK® Model of qZSI

The simulation is done for 3.0 seconds. From $0 \leq t \leq 1.0s$, Case 1 is triggered; from $1.0s < t \leq 2.0s$, Case 2 is triggered; from $2.0 < t \leq 3.0$s, Case 3 is triggered.

A. Parameters Explanation

For this experiment, V_{in} is arbitrarily chosen as 120V and the $D_{sh} = 0.35$ is chosen to yield $V_{dc} = 400V$ based on (1). L and C values are determined using a second-harmonic (2ω) suppression formula, (26) and (27) as proposed in [14]. Variables 'a' and 'b' are the current and voltage ripple ratios respectively. To limit the ripples, the ratios are chosen to be as shown in Table I.

$$L = \frac{aV_{in}(1 - 2D_{sh})}{4\omega bMI_a \cos\varphi} \quad (26)$$

$$C = \frac{MI_a(1 - 2D_{sh})}{a\omega V_{in}} [b\cos\varphi + 1] \quad (27)$$

Hence, using (21) the minimum average inductor current, I_{LB_min} before qZSI enters into DCM can be calculated. Also, based on (11), the average inductor current, I_L for each case with R being varied in 100Ω, 300Ω and 800Ω can be calculated. (Note that since $I_{L1} = I_{L2}$, I_L is used to represent either one to avoid redundancy). The theoretical calculated results clearly are tabulated in Table II.

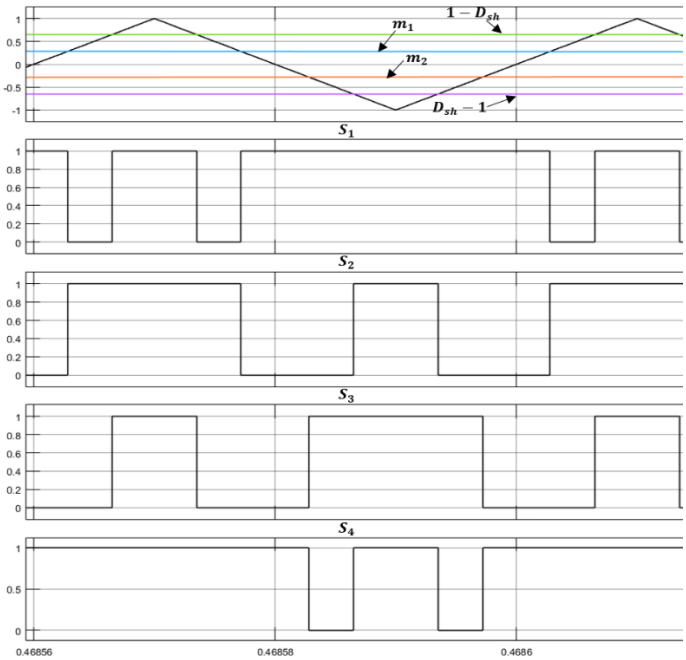

Fig. 7. Simple Boost Control (SBC) using triangular-carrier based SPWM & switching states of all four switches.

TABLE I
SYSTEM PARAMETERS USED FOR SIMULATION

Parameters	Value
Input Voltage, V_{in}	120V
Shoot-through Duty Cycle, D_{sh}	0.35
Modulation Index, M	0.65
DC-link Voltage, V_{dc}	400V
Switching Frequency, f_{sw}	25000Hz
Impedance Angle, θ	0.99
Capacitor-1 voltage, V_{C1}	260V
Capacitor-2 voltage, V_{C2}	140V
Inductance, L ($L_1 = L_2$)	0.000958513H
Capacitance, C ($C_1 = C_2$)	0.000800809F
Current ripple ratio, a	0.000095
Voltage ripple ratio, b	0.0000012
Case 1: Load Resistance, R_1	100Ω
Case 2: Load Resistance, R_2	300Ω
Case 3: Load Resistance, R_3	800Ω

TABLE II
THEORETICAL CALCULATED RESULTS

	Parameters		Theoretical Result		
R (Ω)	L (mH)	C (mF)	V_{dc} (V)	I_{LB_min} (A)	I_L (A)
Case 1: 100	0.959	0.801	400	1.899	5.633
Case 2: 300	0.959	0.801	400	1.899	1.878
Case 3: 800	0.959	0.801	400	1.899	0.704

Notice that in Case 1, $I_L \geq I_{LB\_min}$. qZSI in Case 1 is supposedly to be operating in CCM. In Case 2, $I_L = I_{LB\_min}$. qZSI is supposedly to be operating at the boundary condition. Lastly, in Case 3, $I_L \leq I_{LB\_min}$. Thus, qZSI is hypothesized to be operating in DCM.

Fig. 8 below shows the results obtained from MATLAB/SIMULINK® of V_{dc}, V_{ac} and I_L over the 3.0s span of simulation time.

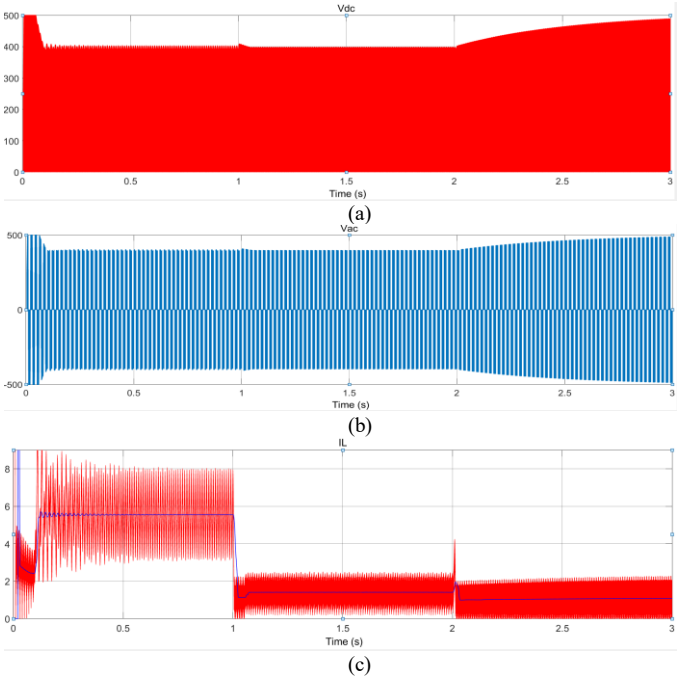

Fig. 8. (a) Simulated waveform of V_{dc}. (b) Simulated waveform of V_{ac} (c) Simulated waveform of I_L over total simulation time.

B. qZSI in CCM

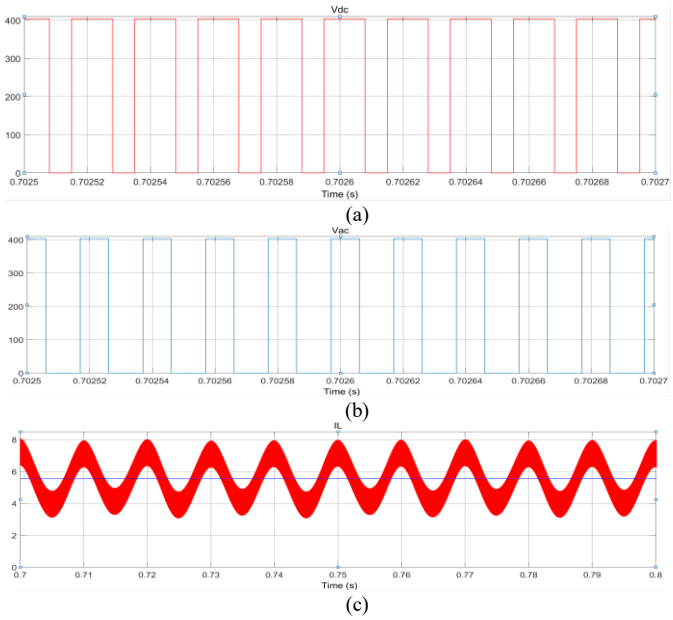

Fig. 9. (a) Simulated waveform of V_{dc} over 0.7025-0.7027s. (b) Simulated waveform of V_{ac} 0.7025-0.7027s. (c) Simulated waveform of I_L over 0.7-0.8s

Simulation results shown in Fig. 9 are taken when qZSI is operating with R = 100Ω as in Case 1 which is in the time span of $0 \leq t \leq 1.0s$. Hence, the results conclude that qZSI is operating in CCM.

C. qZSI at Boundary Condition

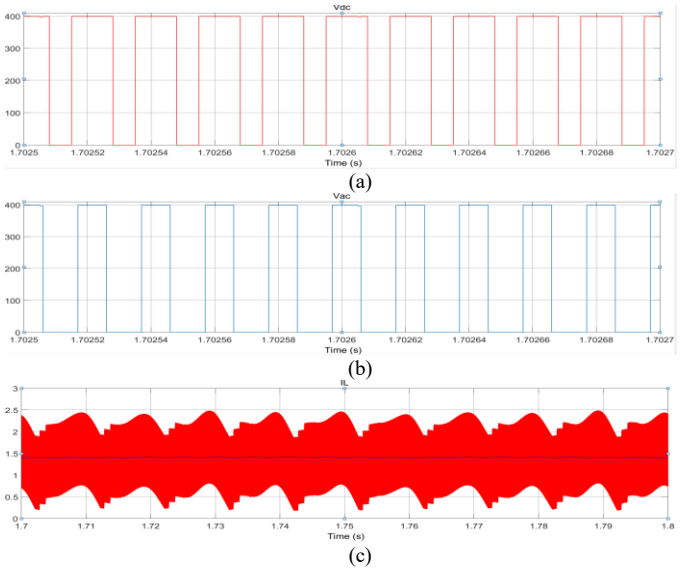

Fig. 10. (a) Simulated waveform of V_{dc} over 1.7025-1.7027s. (b) Simulated waveform of V_{ac} 1.7025-1.7027s. (c) Simulated waveform of I_L over 1.7-1.8s

Simulation results shown in Fig. 10 are taken when qZSI is operating with R = 300Ω as in Case 2 which is in the time span of $1.0s < t \leq 2.0s$. Hence, the results conclude that qZSI is operating at the boundary of CCM and DCM.

D. qZSI in DCM

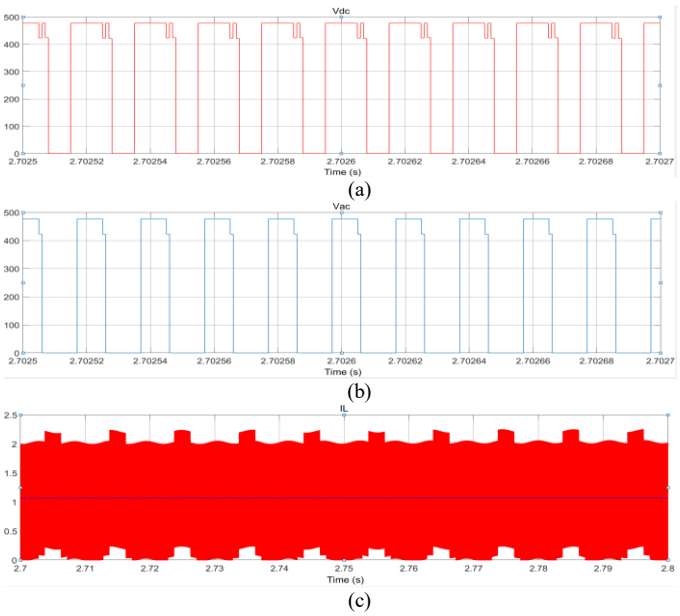

Fig. 11. (a) Simulated waveform of V_{dc} over 2.7025-2.7027s. (b) Simulated waveform of V_{ac} 2.7025-2.7027s. (c) Simulated waveform of I_L over 2.7-2.8s

Simulation results shown in Fig. 11 are taken when qZSI is operating with $R = 800\Omega$ as in Case 3 which is in the time span of $2.0 < t \leq 3.0$s. Hence, the results conclude that qZSI is operating DCM.

E. Results and Discussion

TABLE III
COMPARISON BETWEEN THEORETICAL AND SIMULATED RESULTS

	Theoretical Result			Simulated Result		
R (Ω)	V_{dc} (V)	I_{LB_min} (A)	I_L (A)	V_{dc} (V)	I_{LB_min} (A)	I_L (A)
100	400	1.899	5.633	404	1.899	5.551
300	400	1.899	1.878	400	1.899	1.874
800	400	1.899	0.704	increasing	1.899	increasing

As shown in Table III, when qZSI is operating in CCM as in Case 1, the simulated results are closely tallied with the theoretical results with slight deviation. However, at the boundary condition as in Case 2, the simulated results are almost the same as the theoretical results with negligible deviation. This agrees to the statement above that, the equations governing the operation of qZSI are only valid in CCM. Consequently, the optimal operating condition is near the boundary condition because the simulated results are more precise and accurate.

Besides, in DCM as in Case 3, the obtained simulated results show that qZSI is operating in the region where the CCM steady-state formulae no longer hold. In fact, referring to the derived DCM equation of the qZSI in (23), notice that the term under the square root is always negative. This shows that there is an exponential term in the equation. Hence, this is validated by the simulated result in Fig. 7(a) where as shown, the V_{dc} obtained in DCM region is exponentially increasing.

IV. CONCLUSION

This paper presents a comprehensive analysis of a qZSI operating in CCM and DCM. Mathematical equations are meticulously derived based on valid working principles of the qZSI. Finally, the boundary between CCM and DCM is discovered and technique to avoid qZSI being operated in DCM is also discovered. To verify the derived equations, a qZSI model is being simulated using MATLAB/SIMULINK®. A set of system parameters are determined and the results obtained from the simulation are proven positive. Consequently, the hypothesis of the experiment is accepted; mathematical derivations of CCM and DCM operation of the qZSI are valid.

ACKNOWLEDGMENT

Immense gratitude to Dr. Law Kah Haw for guiding and advising me throughout this project. This work was financially supported by the members of my family, Mr. Ong Eng Keng and Mrs. Yeam Shin Lin.

V. REFERENCES

[1] Y. Liu, H. Abu-Rub and B. M. Ge, "Z-Source / Quasi-Z-Source Inverters," *IEEE Industrial Electronics Magazine* , pp. 32-44, 2014.

[2] I. Roasto and D. Vinnikov, "Analysis and Evaluation of PWM and PSM Shoot-Through Control Methods for Voltage-Fed qZSI based DC/DC Converters," *14th International Power Electronics and Motion Control Conference, EPE-PEMC* , pp. 100-105, 2010.

[3] D. Vinnikov and R. Strzelecki, "Step-Up DC/DC Converters With Cascaded Quasi-Z-Source Network," *IEEE Transactions On Industrial Electronics* , vol. 59, no. 10, pp. 3727-3736, 2012.

[4] Y. Li, S. Jiang, J. G. Cintron-Riverva and Z. P. Fang, "Modeling and Control of Quasi-Z-Source Inverter for Distributed Generation Applications," *IEEE Transactions on Industrial Electronics,* vol. 60, no. 4, pp. 1532-1541, 2013.

[5] N. Sabeur, S. Mekhilef, M. Nakaoka and A. Masaoud, "A Simple Modulation Based Maximum Boost Control Strategy for Three-Phase Quasi-Z-Source Inverter," *2016 IEEE 8th International Power Electronics and Motion Control Conference (IPEMC-ECCE Asia),* pp. 570-574, 2016.

[6] H. Rostami and D. Khaburi, "Voltage Gain Comparison of Different Control Methods of the Z-Source Inverter," *2009 International Conference on Electrical and Electronics Engineering - ELECO 2009,* pp. I-268 - I-272, 2009.

[7] Y. Li, F. Z. Peng, J. G. Cintron-Rivera and S. Jiang, "Controller design for quasi-Z-source inverter in photovoltaic systems," *2010 IEEE Energy Conversion Congress and Exposition,* pp. 3187-3194, 2010.

[8] J. Anderson and F. Z. Peng, "Four Quasi-Z-Source Inverters," *2008 IEEE Power Electronics Specialists Conference,* pp. 2743-2749, 2008.

[9] D. Vinnikov, I. Roasto, R. Strzelecki and M. Adamowicz, "CCM and DCM operation analysis of cascaded quasi-Z-source inverter," *2011 IEEE International Symposium on Industrial Electronics,* pp. 159-164.

[10] L. S. F. and K. A. M. , "A Simple Digital DCM Control Scheme for Boost PFC Operating in Both CCM and DCM," *IEEE Transactions on Industry Applications,* vol. 47, pp. 1802-1812, 2011.

[11] D. A. , J. J. and R. T. D. , "Numerical state-space average-value modeling of PWM DC-DC converters operating in DCM and CCM," *IEEE Transactions on Power Electronics,* vol. 21, pp. 1003-1012, 2006.

[12] K. A. and S. R. K. , "Power loss calculation of diode assisted cascaded Quasi-Z-source converter with CCM and DCM operation," *IEEE 6th International Conference on Power Systems (ICPS),* pp. 1-6, 2016.

[13] Texas Instruments Incorporated, "Understanding Buck Power Stages in Switchmode Power Supplies," Texas Instruments, Texas, USA, 1999.

[14] D. Sun, B. Ge, X. Yan, D. Bi, H. Zhang, Y. Liu, H. Abu-Rub, L. Ben-Brahim and F. Z. Peng, "Modeling, Impedance Design, and Efficiency Analysis of Quasi-Z Source Module in Cascaded Multilevel Photovoltaic Power System," *IEEE Transactions on Industrial Electronics,* vol. 61, no. 11, pp. 6108-6117, 2014.